A scheme for multisource interior tomography

Ge Wang[a] and Hengyong Yu[b]
Biomedical Imaging Division, VT-WFU School of Biomedical Engineering and Sciences, Virginia Tech., Blacksburg, Virginia 24061

Yangbo Ye[c]
Department of Mathematics, University of Iowa, Iowa City, Iowa 52242

(Received 12 January 2009; revised 14 May 2009; accepted for publication 22 May 2009; published 6 July 2009)

Currently, x-ray computed tomography (CT) requires source scanning so that projections can be collected from various orientations for image reconstruction. Limited by the scanning time, the temporal resolution of CT is often inadequate when rapid dynamics is involved in an object to be reconstructed. To meet this challenge, here the authors propose a scheme of multisource interior tomography for ultrafast imaging that reconstructs a relatively small region of interest (ROI). Specifically, such a ROI is irradiated in parallel with narrow x-ray beams defined by many source-detector pairs for data acquisition. This ROI can be then reconstructed using the interior tomography approach. To demonstrate the merits of this approach, the authors report interior reconstruction from *in vivo* lung CT data at a much reduced radiation dose, which is roughly proportional to the ROI size. The results suggest a scheme for ultrafast tomography (such as with a limited number of sources and in a scanning mode) to shorten data acquisition time and to suppress motion blurring. © *2009 American Association of Physicists in Medicine*. [DOI: 10.1118/1.3157103]

Key words: computed tomography (CT), interior tomography, ultrafast tomography, multisource system

I. INTRODUCTION

Since the pioneering works of Hounsfield[1] and Cormack[2] in the past century, x-ray computed tomography (CT) has been widely applied in biomedical applications, nondestructive detection, and so on and has promoted the development of other tomographic modalities such as magnetic resonance imaging, ultrasound tomography, nuclear tomography, and optical molecular tomography. While classic CT theory targets exact reconstruction of a whole cross section or of an entire object from complete projections, practical applications often focus on much smaller internal region of interests (ROIs). Traditional CT methods cannot exactly reconstruct an internal ROI only from truncated projections associated with x-rays through the ROI because this interior problem does not have a unique solution.[3] When applying approximate CT algorithms for interior reconstruction from truncated projection data, features outside the ROI may create artifacts overlapping inside features, rendering the images inaccurate or useless. On the other hand, over the past decades lambda tomography has been developed into a branch of applied mathematics that merely recovers gradientlike features within the ROI from the localized data.[4–9] When applying lambda tomography techniques, the outcomes are not very attractive because of their indirect nature.

Recently, a novel solution for the interior problem was published by our group with numerical results demonstrating for the first time that the interior problem can be solved in a theoretically exact and numerically stable fashion if a small subregion in a ROI is known;[10,11] similar results were also independently reported by other researchers.[12–14] As illustrated in Fig. 1, these findings enable faithful reconstruction of features in a ROI using x-ray beams through the ROI and the linear attenuation coefficient function on a subregion in the ROI.

Closely correlated with the development of CT, higher temporal resolution has been constantly pursued for more demanding needs.[15,16] Although the multisource and multidetector configuration is a natural solution to high temporal resolution CT imaging and already used in the classic Mayo Clinic dynamic spatial reconstructor,[17,18] the modern Siemens dual-source cone-beam scanner,[19] and other tomographic systems,[20] x-ray source scanning remains indispensable. The bulkiness of the detectors in the limited physical space inside a CT gantry makes it impossible to collect a large number of projections simultaneously. Fortunately, with the interior tomography approach, only a ROI needs to be irradiated with a narrower beam, meaning that a much smaller detector can be employed, and many more source-detector pairs can now be assembled into a single system as compared to what is possible previously.

In the following, we extend the interior tomography approach to a scheme of multisource interior tomography for ultrafast imaging of cardiac diseases and other conditions where dynamic imaging and/or high throughputs are important. In Sec. II, we briefly describe our interior tomography approach for what we call "chord averaging." In Sec. III, we report our experimental results based on a sheep CT scan. In Sec. IV, we discuss relevant issues and conclude the paper.

II. CHORD-AVERAGING APPROACH

The key to interior tomography is the inversion of a truncated Hilbert transform (THT). In a 1D model, the THT can be expressed as

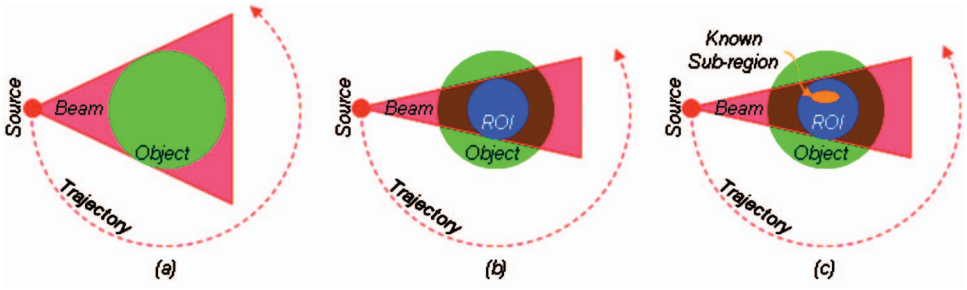

FIG. 1. Interior tomography concept of solving the interior problem. (a) Conventional tomography allows exact reconstruction of an object from a half-scan where every point of the object is irradiated with x-rays from all directions; (b) it was proved impossible to reconstruct uniquely a ROI if only the ROI is irradiated from all the directions (the interior problem); (c) interior problem with a precise knowledge of a sub-region (even small) inside the ROI that can be exactly and stably solved (Ref. 10).

$$g(y) = \frac{1}{\pi}\mathrm{PV}\int_{c_1}^{c_2} f(x)\frac{dx}{y-x} = (H_L f)(y), \quad y \in (c_3, c_4),$$
$$c_1 < c_3 < c_4 < c_2, \tag{1}$$

where "PV" represents the principal value. If there exist real numbers $c_1<c_3<c_5<c_4<c_2$, and $f(x)$ is known on the interval $[c_3,c_5]$, the true value of $f(x)$ can be reconstructed on the interval (c_5,c_4).[10,11] In practice, the 1D function $g(y)$ can be obtained on a generalized PI line/chord by backprojecting the weighted differential projection data, which was first proposed by Gelfand and Graev[21] and rediscovered by Rullgard,[22] Zou and Pan[23,24] as well as Pack *et al.*[25] The importance of these fundamental results is that local projection data are directly linked via the Hilbert transform to the corresponding image to be reconstructed. Once $g(y)$ is known on $[c_3,c_4]$, $f(x)$ can be recovered based on Eq. (1). We adapted a projection-onto-convex-set (POCS) method to reconstruct 1D $f(x)$ iteratively from truncated data $g(y)$ and produced promising numerical results[11] but it was computationally very expensive and sensitive to noise.

On the other hand, the singular value decomposition (SVD) method is a closed-form solution to interior tomography.[26] Our experiments showed that the SVD method was ~200 times faster and produced comparable image quality relative to the POCS method. On a discrete grid, $g(y)$ is sampled along a chord through the known subregion $[c_3,c_4]$ in the ROI as $\mathbf{B}=[b_1,b_2,\ldots,b_P]^T$, and $f(x)$ on the chord as $\mathbf{A}=[a_1,a_2,\ldots,a_Q]^T$. Then, the Hilbert transform is represented as $\mathbf{B}=\mathbf{H}\mathbf{A}$, where $\mathbf{H}$ is a coefficient matrix corresponding to the Hilbert transform kernel.[27] Because $\mathbf{A}$ is partially known, $\mathbf{A}$ can be divided into the known and unknown parts $\mathbf{A}_k$ and $\mathbf{A}_u$. Accordingly, $\mathbf{H}$ is divided into $\mathbf{H}_k$ and $\mathbf{H}_u$. Hence, $\bar{\mathbf{B}}=\mathbf{B}-\mathbf{H}_k\mathbf{A}_k=\mathbf{H}_u\mathbf{A}_u$, which represents a linear inversion problem. Because all the rows of $\mathbf{H}_u$ are formed by the truncated discrete Hilbert transform kernel, one can utilize the properties of $\mathbf{H}_u$ to solve the unknown $\mathbf{A}_u$ from the known $\bar{\mathbf{B}}$. The unknown $\mathbf{A}_u$ includes two parts: part $\mathbf{A}_{ue}$ within the ROI to be exactly reconstructed and part $\mathbf{A}_{un}$ outside the ROI which cannot be exactly recovered. The goal is to ensure that $\mathbf{A}_{ue}$ is reconstructed as precisely and robustly as possible. Without loss of generality, a regularization scheme can be expressed as

$$\hat{\mathbf{A}}_u = \arg\min_{\mathbf{A}_u}(\|\bar{\mathbf{B}}-\mathbf{H}_u\mathbf{A}_u\|^2 + \xi^2\|\mathbf{L}\mathbf{A}_u\|^2), \tag{2}$$

where $\mathbf{L}$ and ξ are a regularization constraint and a weighting parameter, respectively. Our initial SVD solution is to implement the so-called Tikhonov regularization[28] with a unit diagonal constraint matrix $\mathbf{L}$.

It is underlined that the interior tomography reconstruction at a given point can be generally performed along multiple chords through that location. Thus, we propose to utilize this type of data redundancy by appropriately weighting individual 1D-based interior tomography results, transforming the 1D-based reconstruction into a 2D setting for a superior signal-to-noise ratio.

III. EXPERIMENTAL RESULTS

To demonstrate the feasibility of the proposed interior tomography, next we describe a CT experiment with a living sheep, which was approved by Virginia Tech IACUC committee (exempt review). The chest of a sheep was scanned in fan-beam geometry on a SIEMENS 64-slice CT scanner (100 kVp, and 150 mAs). The radius of the x-ray source trajectory was 570 mm. There were 1160 projections uniformly collected over a 360° range and 672 detectors were equiangularly distributed per projection. The radius of the field of view (FOV) was 250.5 mm. First, an entire 290.56 $\times$ 290.56 mm^2 cross section was reconstructed into 1024 $\times$ 1024 pixels using the popular filtered backprojection (FBP) method from complete projections. Second, a trachea (in which we had the perfect knowledge on the CT number of the internal air) was selected in reference to the reconstructed image. Around the trachea, we specified a circular ROI with radius of 120 pixels and kept only the projection data through the ROI. Third, interior tomography of the ROI was performed with the same pixel size as for the global reconstruction on 580 groups of parallel lines through the known trachea region, and these groups were uniformly distributed along the full scan range. Each group included 16 uniformly distributed parallel lines. On each line, we converted the reconstruction problem into a regularization problem in the framework of a truncated Hilbert transform and determined the solution by the SVD.[26,28] Finally, the redundant reconstruction results were averaged to optimize the im-

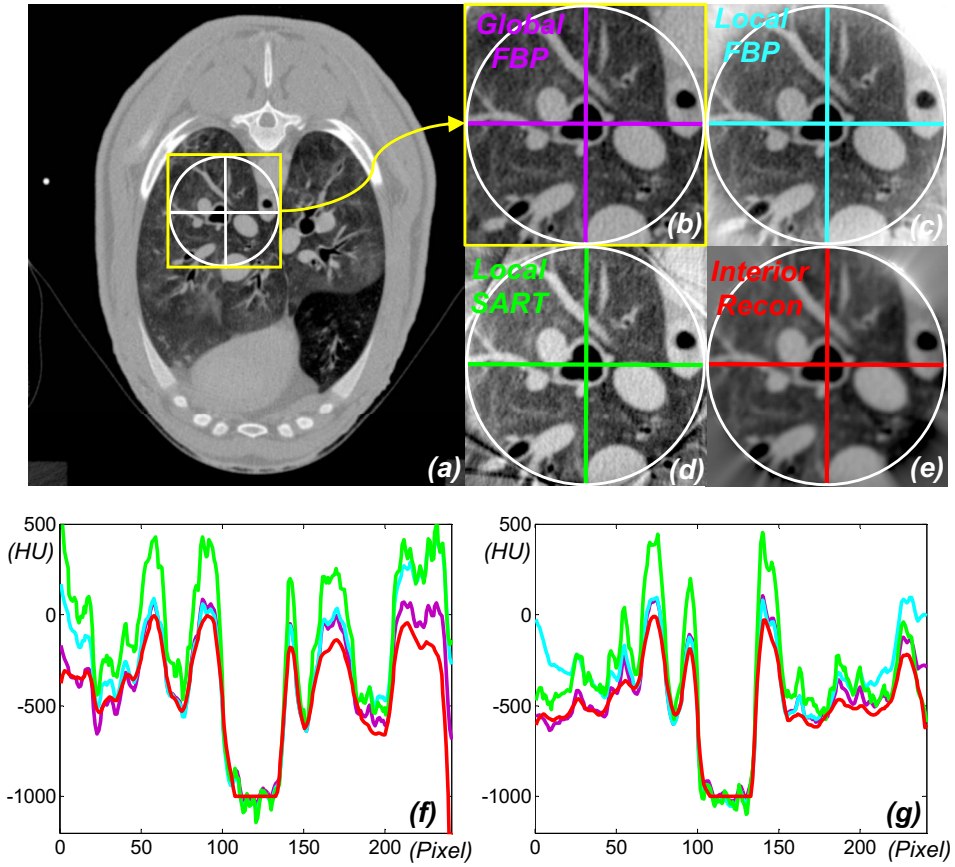

FIG. 2. Demonstration of interior reconstruction with a lung CT scan. (a) The global FBP reconstruction containing a ROI; (b) the magnified ROI in (a); (c) the local FBP (after smooth data extrapolation and optimal constant shift); (d) the local SART (with ordered subsets and optimal constant shift); (e) the local reconstruction via interior tomography; (f) and (g) the color-coded profiles along the horizontal and vertical lines in (b)–(e), respectively. The display window is always [–800HU, 700HU].

age quality. Note that each of the parallel lines in the 580 groups serves as the chord under reconstruction, on which a full-resolution backprojection and filtration (or full-resolution backprojection of differential data) were performed and averaged at each point in the ROI.

Our method produced an excellent ROI reconstruction that was previously impossible and yet ran two orders of magnitude faster than the iterative approach.[11,13] For comparison between our approach and existing approximate local reconstruction algorithms, we adapted the popular FBP algorithm and simultaneous algebraic reconstructive technique (SART).[29] The FBP was applied after the truncated data were sinusoidally extrapolated to zero. The SART was accelerated using the ordered-subset technique (10 subsets and 60 iterations).[29] The representative images and profiles are shown in Fig. 2. Also, we examined key image quality indices of each reconstruction in Fig. 2 using the global FBP reconstruction as the baseline. The results are summarized in Table I. The resolution was statistically estimated orthogonally across the internal borders of the trachea and its nearest disconnected major blood vessel as the full width at half maximum of the line response function fitted into the Gaussian function.[30] The noise was computed as the standard deviation in a flat blood region. Clearly, interior tomography performed much better than either of the competing brute-force algorithms. Surprisingly, it performed even better than the global FBP reconstruction in terms of resolution and noise as we defined in this study most likely because the exact knowledge on the trachea helped regularize interior tomography to yield more favorable resolution and noise in the ROI around the trachea.

Next, let us consider an extreme case of multisource interior tomography based on the aforementioned dataset. Suppose that the x-ray tubes take up no room on the gantry and local projections correspond to detector array segments seamlessly connected, a centralized ROI with radius of 15.4 mm (the gantry is assumed have radius of 570 mm) can be illuminated in parallel from 58 evenly distributed source

TABLE I. Algorithm comparison for interior reconstruction in terms of the mean error $\bar{\varepsilon}$, maximum error ε_{max}, image resolution, and noise. The errors are relative to the global FBP reconstruction.

	$\bar{\varepsilon}$ (HU)	ε_{max} (HU)	Resolution (mm)	Noise (HU)
Global FBP reconstruction	0	0	1.540	34
Local FBP reconstruction	162	440	1.566	49
Local SART reconstruction	199	584	1.538	57
Interior reconstruction	85	439	1.487	21

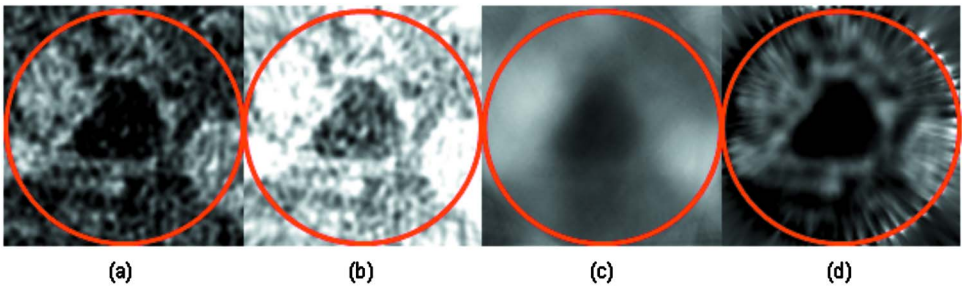

FIG. 3. Demonstration of instant interior reconstruction with a realistic data acquisition setup. The raw data was sampled from the sheep lung scan using only 1 in every 20 projections in the regular full scan. (a) The global FBP reconstruction from the complete data set as a gold standard; (b)–(d) the local reconstructions using the FBP (after smooth data extrapolation), SART (with ordered subsets), and interior tomography techniques, respectively. The display window is [–800HU, 700HU].

positions. These projections were equiangularly selected from the 1160 views by discarding 19 projections in every 20 projections. With the same pixel size as in the above reconstruction, the ROI was of 54 pixels in radius. Then, interior tomography of the ROI was performed on 58 groups of parallel lines, and each group included 22 uniformly distributed parallel lines. The final results are shown in Fig. 3, where the SART result was produced after 200 iterations. Because of the angular downsampling, there are some evident radial streaks in Fig. 3 compared to that in Fig. 2. However, the resultant reconstruction does represent a nearly perfect temporal resolution since these projection data can be acquired in parallel.

IV. DISCUSSIONS AND CONCLUSION

It can be seen in Table I that the image noise level with the global FBP reconstruction is as high as 34 HU, which is much worse than the reported CT scan error of 1 HU on a 20 cm water phantom. This discrepancy is more due to the specific scanning protocol used in this study rather than the inherent accuracy of interior tomography. While we reported an 85 HU error associated with interior tomography in Table I, we have obtained excellent interior reconstructions of physical phantoms, comparable to the global commercial reconstruction in selected ROIs.

For a general CT scan of the heart and the coronary arteries, a FOV of ~150 mm in diameter is preferred (apart from some very special cases where, e.g., only the middle part of the right coronary artery would be of interest) and can be achieved using multisource interior tomography by utilizing a limited number of sources to increase the ROI coverage and scanning the source-detector chains in a circular, spiral-like, or saddlelike trajectories to avoid undersampling, cross scattering, and other issues related to use of too many sources. In the case of $2N+1$ sources, the radius r of the FOV can be maximized by arranging the source-detector pairs equiangularly to reach

$$r = R \sin\left(\frac{\pi}{4N+2}\right), \tag{3}$$

where R is the radius of the scanning circle. According to Eq. (3), the radius of FOV is decreased as the number of sources is increased. Specifically, we can cover a FOV of 162 or 134 mm in diameter with 11-source or 13-source interior tomography architectures, respectively, assuming the imaging geometry $R=570$ mm of a Siemens CT scanner (SOMATOM Volume Zoom, Siemens Medical Solutions USA, Inc., Malvern, PA) used in our laboratory. In these two cases, the temporal resolution will be improved by greater than tenfold and >12-fold, respectively (taking into account the effect of the fan angle which is small in the interior tomography mode), while the image quality remains the same as that shown in Fig. 2. This idea is further illustrated in Fig. 4 assuming use of seven sources. Recently, we published a paper on compressive sensing (CS)-based interior tomography, demonstrating that if an underlying function over a ROI is piecewise constant, then exact interior reconstruction can be achieved via total variation minimization, without precise knowledge on a subregion in the ROI.[31] More specifically, our previously published THT-based interior tomography and newly reported CS-based interior tomography techniques can be contrasted in Table II. In other words, our THT-based interior tomography can handle a general function on a ROI but it needs precise prior knowledge on a subregion in the ROI. On the other hand, our CS-based inte-

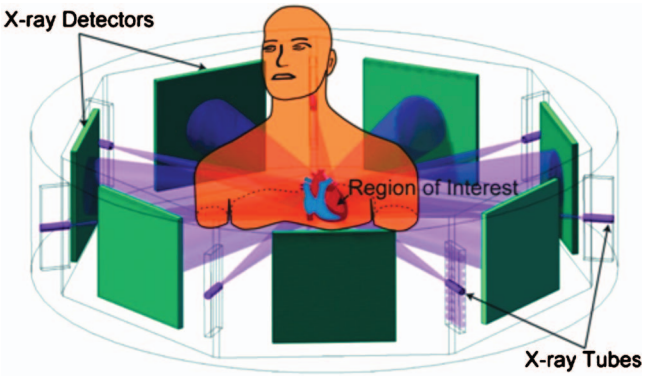

FIG. 4. Multisource interior tomography concept—A typical seven-saddle-curve scanning mode for interior cardiac CT to reduce radiation dose and data acquisition time. With the interior tomography approach, the detector size can be much reduced so that more source-detector pairs can be integrated to focus on a ROI for simultaneous collection of multiple local projections.

TABLE II. Differences between our THT-based and CS-based interior tomography techniques.

	A priori image model	Precise *a priori* knowledge	Computational essence	Angular sampling rate	Current maturity
THT-based interior tomography	Quite general	A subregion	Inversion of truncated Hilbert data	Normal	High
CS-based interior tomography	Piecewise constant	Unnecessary	Minimization of total variation	Potentially low	Low

rior tomography does not need precise knowledge on a subregion in a ROI but it assumes a piecewise constant function on the ROI. For THT-based interior tomography, inversion of THT data is the key. For CS-based interior tomography, the total variation over the ROI is minimized subject to the data constraint and can be implemented using an iterative procedure. Note that a simple minded application of an iterative algorithm such as SART will not produce good results for interior tomography because it is essential to utilize the Hilbert transform constraint and precise knowledge on a subregion for accurate reconstruction of a general function on a ROI, and similarly essential to minimize the total variation for accurate recovery of a piecewise constant function on a ROI without precise subregion knowledge. When an underlying function over a ROI is not piecewise constant, our CS-based interior tomography cannot produce accurate reconstruction; for example, the interior reconstruction from local data of the sheep scan is subject to a background level shift (see Fig. 6 in Ref. 31). A promising futuristic possibility is to combine and extend both THT-based and CS-based methods so that the knowledge/image model requirements can be less restrictive for more general applications.

Exact knowledge on a subregion can often be assumed because in many cases we already know the x-ray linear attenuation coefficients of air gaps or voids, water or other liquids, or other calibrated structures such as implants and substrates; more generally, a prescan may often acquire such prior knowledge. Thus, use of such subregion knowledge can indeed be made for many practical interior reconstruction problems. As another example, locating an air pocket in the lungs is quite doable since airways are not difficult to find in a localized lung scan. It is recognized that the inflowing contrast agent changes the CT numbers not only in the vessels but also in the myocardium and cardiac chambers. In this case, we may have to use spinal and lung features to help interior cardiac CT.[32] Alternatively, we are developing a compressed sensing approach to perform interior tomography based on some weak image model,[31] as discussed above.

Ultrafast tomography is highly desirable in a number of disciplines. We cite three such examples as follows. First, ultrafast tomography may improve cardiac CT. Cardiac CT has emerged as a promising tool for noninvasive coronary angiography.[33] Electron-beam CT was the first dedicated cardiac CT modality with temporal resolution of as low as 50 ms, but it is obsolete because of its major restrictions in spatial and contrast resolution. State-of-the-art medical CT scanners can achieve temporal resolution of 100 ms. However, given the rate and the magnitude of the cardiac motion, temporal resolution should ideally be <10 ms for humans and <2 ms for small animals such as rats and mice.[16] While achieving these resolutions has been extremely challenging, our ultrafast interior tomography approach can help improve the temporal resolution to assess the calcium burden and vascular stenoses, to identify positive remodeling and plaque consistency, especially in the cases of high/irregular heart rates. Second, ultrafast tomography may enable clinical micro-CT such as for inner ear imaging.[15] Two major obstacles in achieving such fine spatial resolution *in vivo* are physiological motion induced blurring (the finer the image resolution, the more significant the physiological motion will be, which is in an order of a millimeter) and radiation dose concern (the finer the resolution, the much greater the radiation dose will be delivered to the patient). When the x-ray beams target a small ROI and projections are acquired in parallel, the above two issues are effectively addressed at the same time, which may help derive ultrafine features of interest (image-based biomarkers) for many applications of diagnosis and therapy. Third, ultrafast interior tomography is the ideal modality for the so-called process tomography, which, for example, might be used for multiphase imaging of the contrast dynamics in the body,[34] or mass flow of oil and water that is pumped from oil reservoirs.[35]

A promising way to suppress image artifacts and/or increase the FOV is to use detectors in a time-sharing fashion which can also be referred to as a source-multiplexing scheme. Similar to the Hadamard multiplexing method developed by Zhang *et al.*,[36] we can arrange $p \times q$ x-ray focal spots around a subject, along with the corresponding detectors. Under the computer control, we can electronically trigger p x-ray sources simultaneously for q times to produce projection data continuously on the associated detectors. In this way, each detector will be used by q x-ray focal spots in q consecutive time slots. Note that this method can not only improve image quality but also avoid the conflict between the ROI size and number of focal spots that are on at the same time. While this multiplexing scheme is not instant, it can acquire a complete dataset at speed one to two orders of magnitude faster for a relatively small ROI than that of the state-of-the-art CT scanner.

While the presented results showing the feasibility of interior tomography are quite encouraging, a critical examination indicates that the current interior tomography technol-

ogy is not perfect yet, as evidenced by the lack of details and residual artifacts in the peripheral region in Fig. 2(e) as compared to that in Fig. 2(b). This suboptimal performance is due to the fact that the stability analysis of the current interior tomography technique reveals that the reconstruction error would increase further away from the subregion on which we have exact knowledge. Actually, both tremendous biomedical imaging needs for interior tomography and this type of flaws in image quality with interior tomography indicate opportunities to advance this new area and capitalize its major benefits in clinical and preclinical applications.

One may worry that the scatter with this multisource system would be extremely high. Actually, this is not necessarily the case.[37,38] Briefly speaking, the larger the number of sources (which is typically odd) we want to use, the narrower each x-ray beam we should make, and the smaller the field of view we will have. Clearly, the scatter in the data is roughly proportional to the product of the number of simultaneously active sources and the beam width (which is proportional to the size of the field of view). Thus, the scatter to primary ratio can be controlled to be practical. Also, detector collimation can be used to reject scattered photons.

In conclusion, interior tomography enables ultrafast imaging performance utilizing (1) prior knowledge on a small spot in the ROI or a weak image model such as ROI being piecewise constant and (2) multiple narrow-beam-oriented source-detector pairs. Briefly speaking, interior tomography is advantageous to reduce radiation dose (no x-rays go outside a ROI), suppress scattering artifacts (no cross-talk from radiation outside the ROI), refine image quality (with the new reconstruction approach and prior knowledge), handle large objects (measurement can be localized in any direction, assuming a centralized ROI or dynamic x-ray collimation), and can be extended to some other tomographic modalities such as for multisource interior SPECT.[39] We believe that this novel tomographic approach will have significant biomedical applications.

ACKNOWLEDGMENTS

This work was partially supported by NIH under Grant Nos. EB002667, EB004287, and EB007288. The authors thank Ms. Cyndy Williams for editorial refinements, Dr. Harry Shen for drawing Fig. 4, the editors, reviewers, and Dr. Alexander Katsevich for helpful comments, Dr. Erik Ritman (Mayo), Dr. Zhenxue Jiang (Hologic), and Dr. Otto Zhou (University of North Carolina), and Bruno De Man (GE Global Research) for discussions on sources and detectors. The sheep lung dataset was from Dr. Eric Hoffman, University of Iowa, when the first author was in collaboration with Dr. Hoffman on his NIH Project No. HL064368.

[a]Electronic mail: wangg@vt.edu
[b]Electronic mail: hengyongyu@vt.edu
[c]Electronic mail: yangbo-ye@uiowa.edu

[1]G. N. Hounsfield, "Computerized transverse axial scanning (tomography). Part I. Description of system," Br. J. Radiol. **46**, 1016–1022 (1973).
[2]A. M. Cormack, "Representation of a function by its line integrals with some radiological applications," J. Appl. Phys. **34**(9), 2722–2727 (1963).
[3]F. Natterer, *The Mathematics of Computerized Tomography*, Classics in Applied Mathematics (Society for Industrial and Applied Mathematics, Philadelphia, 2001).
[4]A. Faridani *et al.*, "Local tomography II," SIAM J. Appl. Math. **57**(4), 1095–1127 (1997).
[5]A. Faridani, E. L. Ritman, and K. T. Smith, "Local tomography," SIAM J. Appl. Math. **52**, 459–484 (1992).
[6]A. G. Ramm and A. I. Katsevich, *The Radon Transform and Local Tomography*, (CRC, Boca Raton, FL, 1996).
[7]H. Y. Yu, Y. C. Wei, Y. B. Ye, and G. Wang, "Lambda tomography with discontinuous scanning trajectories," Phys. Med. Biol. **52**(14), 4331–4344 (2007).
[8]E. T. Quinto, "Local algorithms in exterior tomography," J. Comput. Appl. Math. **199**(1), 141–148 (2007).
[9]E. T. Quinto and O. Oktem, "Local tomography in electron microscopy," SIAM J. Appl. Math. **68**(5), 1282–1303 (2007).
[10]G. Wang, Y. B. Ye, and H. Y. Yu, "General VOI/ROI reconstruction methods and systems using a truncated Hilbert transform," Patent No. 60/989,591 (15 May 2007).
[11]Y. B. Ye, H. Y. Yu, Y. C. Wei, and G. Wang, "A general local reconstruction approach based on a truncated Hilbert transform," Int. J. Biomed. Imaging **2007**, 63634 (2007).
[12]M. Courdurier *et al.*, "Solving the interior problem of computed tomography using a priori knowledge," Inverse Probl. **24**, 065001 (2008).
[13]H. Kudo *et al.*, "Tiny a priori knowledge solves the interior problem," in 2007 IEEE Nuclear Science Symposium Conference pp. 4068–4075.
[14]H. Kudo *et al.*, "Tiny a priori knowledge solves the interior problem in computed tomography," Phys. Med. Biol. **53**(9), 2207–2231 (2008).
[15]G. Wang *et al.*, "Design, analysis and simulation for development of the first clinical micro-CT scanner," Acad. Radiol. **12**(4), 511–525 (2005).
[16]G. Wang *et al.*, "Top-level design and preliminary physical analysis for the first electron-beam micro-CT scanner," J. X-Ray Sci. Technol. **12**(4), 251–260 (2004).
[17]R. A. Robb *et al.*, "High-speed three-dimensional x-ray computed tomography: The dynamic spatial reconstructor," Proc. IEEE **71**(3), 308–319 (1983).
[18]E. L. Ritman, R. A. Robb, and L. D. Harris, *Imaging Physiological Functions: Experience with the DSR* (Praeger, Philadelphia, 1985).
[19]T. G. Flohr *et al.*, "First performance evaluation of a dual-source CT (DSCT) system," Eur. Radiol. **16**(2), 256–268 (2006).
[20]Y. Liu *et al.*, "Half-scan cone-beam CT fluoroscopy with multiple x-ray sources," Med. Phys. **28**(7), 1466–1471 (2001).
[21]I. M. Gelfand and M. I. Graev, "Crofton function and inversion formulas in real integral geometry," Funct. Anal. Appl. **25**(1), 1–5 (1991).
[22]H. Rullgard, "An explicit inversion formula for the exponential Radon transform using data from 180 ∼," Ark. Mat. **42**, 353–362 (2004).
[23]Y. Zou and X. C. Pan, "An extended data function and its generalized backprojection for image reconstruction in helical cone-beam CT," Phys. Med. Biol. **49**(22), N383–N387 (2004).
[24]Y. Zou and X. C. Pan, "Exact image reconstruction on PI-lines from minimum data in helical cone-beam CT," Phys. Med. Biol. **49**(6), 941–959 (2004).
[25]J. D. Pack, F. Noo, and R. Clackdoyle, "Cone-beam reconstruction using the backprojection of locally filtered projections," IEEE Trans. Med. Imaging **24**(1), 70–85 (2005).
[26]H. Y. Yu, Y. B. Ye, and G. Wang, "Local reconstruction using the truncated Hilbert transform via singular value decomposition," J. X-Ray Sci. Technol. **16**(4), 243–251 (2008).
[27]H. Y. Yu and G. Wang, "Studies on implementation of the Katsevich algorithm for spiral cone-beam CT," J. X-Ray Sci. Technol. **12**(2), 96–117 (2004).
[28]P. C. Hansen, "Truncated singular value decomposition solutions to discrete ill-posed problems with ill-determined numerical rank," SIAM (Soc. Ind. Appl. Math.) J. Sci. Stat. Comput. **11**(3), 503–518 (1990).
[29]G. Wang and M. Jiang, "Ordered-subset simultaneous algebraic reconstruction techniques (OS-SART)," J. X-Ray Sci. Technol. **12**(3), 169–177

(2004).
[30]F. J. Schlueter *et al.*, "Longitudinal image deblurring in spiral Ct," Radiology **193**(2), 413–418 (1994).
[31]H. Y. Yu and G. Wang, "Compressed sensing based Interior tomography," Phys. Med. Biol. **54**(9), 2791–2805 (2009).
[32]D. Bharkhada *et al.*, "Cardiac CT radiation dose reduction using interior reconstruction algorithm using the aorta and vertebra as known information," J. Comput. Assist. Tomogr. **33**(3), 338–347 (2009).
[33]M. Naghavi *et al.*, "From vulnerable plaque to vulnerable patient—A call for new definitions and risk assessment strategies: Part I," Circulation **108**(14), 1664–1672 (2003).
[34]G. Wang, G. Schweiger, and M. W. Vannier, "An iterative algorithm for x-ray CT fluoroscopy," IEEE Trans. Med. Imaging **17**(5), 853–856 (1998).
[35]E. J. Morton *et al.*, "Development of a high speed x-ray tomography system for multiphase flow imaging," IEEE Trans. Nucl. Sci. **46**(3), 380–384 (1999).
[36]J. Zhang *et al.*, "Hadamard multiplexing radiography based on carbon nanotube field emission multi-pixel x-ray technology," Proc. SPIE **6913**, 69131T (2008).
[37]A. Ahnesjo *et al.*, "Beam modeling and verification of a photon beam multisource model," Med. Phys. **32**(6), 1722–1737 (2005).
[38]J. Zhao, Y. N. Jin, Y. Lu, and G. Wang, "A filtered backprojection algorithm for triple-source helical cone-beam CT," IEEE Trans. Med. Imaging **28**(3), 384–393 (2009).
[39]H. Y. Yu, J. S. Yang, M. Jiang, and G. Wang, "Interior SPECT-Exact and stable ROI reconstruction from uniformly attenuated local projections," Commun. Numer. Methods Eng. **25**(6), 693–710 (2009).